remote sensing

MDPI

Article

Intelligent Monitoring Applications of Landslide Disaster Knowledge Graphs Based on ChatGLM2

Zhengrong Wu [1], Haibo Yang [1,*], Yingchun Cai [1], Bo Yu [2], Chuangheng Liang [1], Zheng Duan [3] and Qiuhua Liang [1]

[1] School of Water Conservancy and Transportation, Zhengzhou University, Zhengzhou 450001, China
[2] CEC Guiyang Exploration and Design Research Institute Co., Guiyang 550081, China
[3] Department of Physical Geography and Ecosystem Science, Lund University, S-22362 Lund, Sweden
* Correspondence: yanghb@zzu.edu.cn

Abstract: Over the years, the field of landslide disaster research has amassed a wealth of data and specialized knowledge. However, these resources originate from a wide array of sources and often feature complex data structures, highlighting a persistent lack of methods to integrate multi-source, heterogeneous data. Traditional landslide monitoring methods typically focus on singular monitoring targets and data sources, which limits a comprehensive understanding of the complex processes involved in landslides. This paper introduces a landslide monitoring model based on a knowledge graph. This model employs P-Tuning to fine-tune ChatGLM2 for the extraction of triples. Differential InSAR (D-InSAR) is utilized to extract ground deformation data, which is then integrated with the knowledge graph for landslide monitoring and analysis. This study focuses on the co-seismic landslide in Jishishan, Gansu, China. By analyzing the landslide knowledge graph and the spatiotemporal deformation map, the results are as follows: (1) For this event, 106 entities and attributes were constructed, along with two recommended calculation routes. (2) The deformation at the earthquake's central region reached up to 8.784 cm, with a slightly smaller deformation zone to the northwest peaking at 9.662 cm. Significant unilateral subsidence was observed in the mountain range to the southwest. (3) The area affected by the co-seismic landslide primarily includes farmland and villages, covering an area of 0.3408 square kilometers. (4) Analysis based on the knowledge graph indicates that this landslide was primarily caused by the rapid liquefaction of water-saturated soil layers due to the earthquake, resulting in instability. This study contributes to the analysis of post-disaster losses, attribution, and impacts.

Keywords: multi-source heterogeneous data; expert knowledge formalization; spatio-temporal knowledge inference; disaster monitoring

check for updates

Citation: Wu, Z.; Yang, H.; Cai, Y.; Yu, B.; Liang, C.; Duan, Z.; Liang, Q. Intelligent Monitoring Applications of Landslide Disaster Knowledge Graphs Based on ChatGLM2. *Remote Sens.* **2024**, *16*, 4056. https://doi.org/10.3390/rs16214056

Academic Editors: Adrian Ursu, Cristian Constantin Stoleriu and Marian Mierlă

Received: 20 September 2024
Revised: 29 October 2024
Accepted: 29 October 2024
Published: 31 October 2024

Copyright: © 2024 by the authors. Licensee MDPI, Basel, Switzerland. This article is an open access article distributed under the terms and conditions of the Creative Commons Attribution (CC BY) license (https://creativecommons.org/licenses/by/4.0/).

1. Introduction

Over the past few decades, the frequency and complexity of natural disasters have continuously increased [1–3], due to global climate change [4] and environmental degradation [5–7], posing severe challenges to human societies. Significant catastrophic events, such as the Wenchuan earthquake, the Southern snow disaster, and the Beijing "7.21" torrential rain, have not only caused substantial economic losses but have also severely impacted the safety and quality of life of the people [8–10]. According to the Global Landslide Database, between 2007 and 2013, landslides resulted in the deaths of over 20,500 individuals across 1827 events [11]. Against this backdrop, disaster management and emergency response have become pressing issues of concern [12].

Landslides, in particular, occur frequently in China, ranking among the highest globally [13]. Their complex mechanisms, sudden onset, and unpredictable spatio-temporal characteristics make them a significant hazard, posing a serious threat to lives and property. A landslide refers to the downhill movement of earth and rock masses along a defined

sliding surface under gravity. As one of the major natural hazards, landslides cause significant direct and indirect property damage annually [14]. In China, landslide disasters have resulted in a total death toll exceeding 5000 people, with annual economic losses estimated at 500 million yuan due to landslides [15]. To effectively address the challenges posed by landslide disasters, academia and the practical fields have conducted extensive research aimed at exploring the intrinsic patterns, evolutionary mechanisms, and emergency management strategies of landslide disasters. In recent years, the rapid development of information technology, especially the widespread application of emerging technologies such as artificial intelligence, big data, cloud computing, knowledge graphs, and geographic information systems, has provided new ideas and tools for landslide disaster management [16–18]. Among various technologies, knowledge graphs have demonstrated great potential in handling and analyzing complex data [19,20]. Decision-makers or researchers faced with vast knowledge bases often struggle to quickly extract and analyze relevant information. Knowledge graphs transform data into interconnected knowledge entities and relationships, offering an intuitive and efficient way to organize and browse information [21,22], significantly enhancing the efficiency of information retrieval and knowledge mining [23,24]. The construction of knowledge graphs is based on vast amounts of knowledge data [25]. These data sources, such as weather reports, geographic information, social media updates, satellite images, and historical disaster records, pose considerable challenges due to their heterogeneity, inconsistency, and incompleteness [26,27]. Although previous studies have aimed to address the heterogeneity issues among various disaster data [28,29], they are limited by the scope of data studied, making it difficult to match new data sources to existing rules. The timeliness of obtaining and utilizing key data or resources related to landslide risk remains a challenge. Knowledge graphs use entities and relationships to connect and structurally store massive amounts of heterogeneous data, enabling deep analysis by understanding and representing the semantic connections between data [30,31].

An essential part of constructing a knowledge graph is the extraction of entities and relationships. The multi-source nature of landslide disaster data makes relationship extraction and modeling particularly challenging. Traditional extraction methods often utilize pattern matching and dependency parsing [32]. These methods rely on strict grammatical rules and prior knowledge, yet the data associated with landslide incidents often comes from diverse sources such as social media, news reports, and official announcements, which can vary significantly in format and style. Traditional methods, dependent on strict grammatical rules and prior knowledge, typically perform poorly with this diverse and unstructured text [33]. With the advancement of large language models, relationship extraction methods based on these models have shown significant advantages in handling unstructured data. Through extensive pre-training, large language models are able to learn a wealth of linguistic knowledge and semantic information across a wide range of corpora [34,35]. This enables them to adapt flexibly to the multi-source and heterogeneous nature of landslide disaster data. Such models can effectively extract and interpret complex relationships and entities from varied data sources, enhancing the accuracy and comprehensiveness of the knowledge graphs they help to build.

Traditional landslide monitoring methods can be broadly classified into ground observation techniques, remote sensing technologies, and geological investigation methods. Ground observation techniques include visual inspection, where personnel conduct periodic surveys to observe the development of cracks, displacement, and hydrological conditions in landslide-prone areas [36]. This approach is cost-effective and straightforward, but its accuracy may be affected by the subjectivity of observers and the limited frequency of inspections. With technological advancements, instruments such as inclinometers and leveling devices have been employed to monitor the tilt and settlement of soil or rock masses, improving the precision and reliability of measurements [37]. However, these instruments may be constrained by adverse weather conditions or complex terrains. Crack meters and similar devices are commonly used to monitor the expansion and rate of cracks, providing

continuous data, though their installation and maintenance can be expensive. Since the mid-19th century, remote sensing technology has developed rapidly. Some studies use satellite imagery to monitor landslides by analyzing changes in surface features [38]. While remote sensing can cover large areas and rapidly acquire vast amounts of data, the quality of data may be limited by sensor capabilities, cloud cover, and resolution. Moreover, it is challenging to monitor landslide sites in detail using visible light spectrum combinations, and ground-based data are still needed for support. Interferometric Synthetic Aperture Radar (InSAR) technology, an advanced method that uses radar waves to measure surface deformation, provides a precise means of detecting subtle surface displacements over large areas, offering an effective tool for landslide monitoring. However, its application is limited by high costs and technical complexity [39]. Geological investigation methods, such as borehole detection, ground-penetrating radar, and geological mapping, are used to analyze the geological structure and physical properties of landslide areas in depth, helping to identify potential landslide risks [40]. These methods can provide detailed subsurface information, but they are often time-consuming and expensive. Traditional landslide monitoring models typically rely on specific datasets from geology, meteorology, and environmental factors [41,42]. These data are often isolated and managed in a fragmented manner, leading to low efficiency in data integration and utilization, and may not fully leverage all relevant data. Most traditional models are designed for specific regions and types of data, and their applicability and accuracy may decline when environmental conditions or data sources change [43]. Moreover, in facing complex disaster chains, traditional analysis methods may overlook the interactions between different disasters [44]. Knowledge graphs, as a form of specialized graph database, represent a transformative tool in landslide monitoring and risk assessment. Unlike traditional monitoring methods that often rely on isolated data sets from specific domains such as geology, meteorology, or environmental conditions, knowledge graphs enable the integration of multi-source data along with expert knowledge into a structured and cohesive knowledge base [45]. This comprehensive integration facilitates a more profound and extensive analysis of landslide risks, which traditional methods struggle to achieve. One of the key advantages of using knowledge graphs is their ability to perform associative analysis and reasoning mechanisms. These capabilities allow the system to uncover hidden relationships between various data points that may not be apparent in traditional models [46]. Therefore, models based on knowledge graphs can more comprehensively analyze landslide risks.

Given the challenges identified in landslide disaster monitoring research, there is an urgent need for a more comprehensive and timely monitoring model for landslide disasters. Therefore, (1) this study proposes an intelligent knowledge graph construction method based on ChatGLM2 [47] and uses this model in conjunction with ontological theory to build a landslide knowledge graph. This approach addresses the difficulties of integrating unstructured data with ontological theory to provide structured expressions. (2) Based on the constructed landslide knowledge graph, we have developed a knowledge graph-based landslide disaster inference model. This model facilitates spatio-temporal monitoring of landslide disasters and addresses the inefficiencies of traditional monitoring through an automated workflow. This novel approach enhances the predictive capabilities and response times of landslide monitoring systems, ultimately contributing to more effective disaster management and mitigation strategies.

2. Data and Methods

2.1. Study Area

The epicenter of the Jishishan earthquake and the location of the Jishishan co-seismic landslide are shown in Figure 1. Jieshishan is located in Jieshishan An Dongxiang Salar Autonomous County, which belongs to Linxia Hui Autonomous Prefecture of Gansu Province. The county where Jieshi Mountain is located has a total area of 909.97 square kilometers, with a resident population of 238,900. Jishishan County is located in a typical continental monsoon climate zone, exhibiting the combined climatic features of mountainous and

alpine regions, with significant climatic variations across the county due to topographical influences. The average annual precipitation is 651.1 mm, while the average annual evaporation is approximately 1114 mm. The total annual sunshine duration is 1754.2 h, and the frost-free period ranges from 113 to 177 days. The winter and spring seasons are dry, whereas the summer and autumn seasons are humid. There are five rivers originating from the Lesser Jishi Mountain within the county, among which the Liuji River has the largest drainage area and flow rate. The region is located in a loess area, characterized by a macroporous, metastable microstructure and strong water sensitivity. Its lithology is primarily composed of eolian deposits and limestone, while the predominant soil types are Gleyic Cambisols and Aric Anthrosols. At 23:59 GMT on 18 December 2023, a magnitude 6.2 earthquake struck near Jieshishan (35.70 degrees north latitude, 102.79 degrees east longitude) and triggered a syncline in Jieshishan.

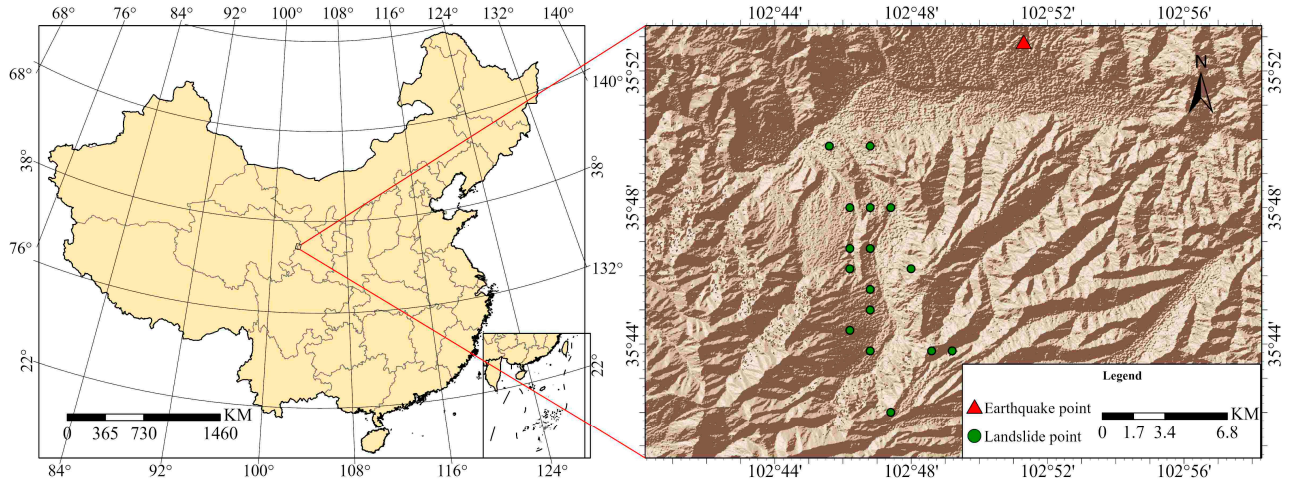


Figure 1. Locations of the landslide and earthquake points in Jishishan. The (**left**) side shows a map of China, while the (**right**) side displays the area under study.

2.2. Data Source

This study utilizes data from three sources. The literature data were sourced from China National Knowledge Infrastructure (https://www.cnki.net/, accessed on 25 August 2024) using the keywords "Jishishan landslide", comprising 39 documents with a total of 1,159,985 characters. Public reporting data were collected from Weibo (https://weibo.com/, accessed on 25 August 2024) and Zhihu (https://www.zhihu.com/, accessed on 25 August 2024) using the keywords "Jishishan landslide", amounting to 842 posts and 170,960 characters, and disaster statistics section of the China National Disaster Reduction Center's website (https://www.ndrcc.org.cn/, accessed on 25 August 2024), totaling 44 entries with 86,958 characters. The statistical results are presented in Table 1.

Table 1. Data volume from each source.

Source	Number of Entries (Posts, Articles)	Number of Characters
Literature	39	1,159,985
Public reporting	886	257,918

Sentinel-1 is the first satellite launched as part of a collaboration between the European Space Agency (ESA) and the Copernicus Programme. It consists of two similar satellites, Sentinel-1A and Sentinel-1B, launched in 2014 and 2016, respectively. Under the Interferometric Wide Swath (IW) mode, Sentinel-1 provides a resolution of approximately 5 m (azimuth) by 20 m (range). Equipped with a C-band Synthetic Aperture Radar (SAR), Sentinel-1 can detect even very minute ground movements, aiding in the assessment of

landslide activity and trends. Sentinel-2, also part of ESA's Copernicus Programme, is specifically designed for monitoring Earth's environment and managing natural resources. The Sentinel-2 satellite system includes Sentinel-2A and Sentinel-2B, launched in 2015 and 2017, respectively. Their orbital configuration enables them to cover the globe every five days, ensuring the availability of timely data. Sentinel-2 is equipped with a high-resolution multispectral imager that captures images in 13 spectral bands, covering visible, near-infrared, and short-wave infrared frequencies. This design makes it particularly suitable for monitoring landslide disasters. The imagery used in this case study is listed in Table 2.

Table 2. Details of remote sensing imagery data used in the study.

Data Name	Data ID		Tile Number	Acquisition Time	Spatial Resolution (m)	Data Source
	Path	Frame				
Sentinel-1	135	473	--	14 December 2023	5 × 20	https://dat%C2%B7aspace.copernicus.eu, accessed on 25 August 2024
Sentinel-1	135	473	--	26 December 2023	5 × 20	
Sentinel-2	--	--	T48SUE	20 December 2023	10	
Sentinel-2	--	--	T48STE	8 December 2023	10	

2.3. Landslide Monitor Model

To address the heterogeneity and inconsistency of multi-source data, we have implemented detailed standardization steps during the data preprocessing phase, including data format conversion, unification of time and spatial coordinates, imputation of missing values, and data cleaning. Additionally, data mapping and semantic alignment methods are employed to ensure compatibility and consistency across different data sources. The monitoring module continuously tracks feature data, including precipitation and seismic information. If anomalies are detected, the system queries the Neo4j graph database and retrieves additional data for model computation, ultimately providing auxiliary data for research. The overall structure of the monitoring model is illustrated in Figure 2. A knowledge graph monitoring model for landslide prediction involves utilizing station network interfaces to process and align multiple data sources in bulk before storing them in a database. The model will periodically query interfaces from multiple data stations. For data with provided signatures, the model checks the local database; if the data does not exist, it proceeds with the storage step. For data without provided signatures, the MD5 (Message Digest Algorithm 5) is used to obtain a hash value of the specified data. If the data exists in the database, it is discarded; otherwise, it proceeds to the storage step. The storage step primarily includes ontology alignment and data storage. In the ontology alignment stage, data from different sources are embedded into the ontology based on predefined mapping files. During the storage stage, py2neo is used for database connection and data storage. For unstructured data, a random subset is initially selected to construct question-answer templates. This data is input into ChatGLM-130B to obtain preliminary triplets, which are then manually filtered to retain the correct triplets. Detailed methodology is described in Section 2.3.2. These texts and triplets are used as training data for ChatGLM2-6B to obtain the model weight file. The model weight file is loaded into ChatGLM2-6B, and the entire dataset from the data sources is input into the model to obtain triplets, which are subsequently imported into the Neo4j graph database. The monitoring module continuously monitors feature data, including precipitation and seismic information. If anomalies are detected, it queries the Neo4j graph database and retrieves additional data for model computation, ultimately providing auxiliary data for research. Through these detailed methods for standardizing and processing multi-source data, the model is able to more effectively integrate and analyze heterogeneous data from various sources, enhancing the accuracy and timeliness of landslide disaster monitoring.

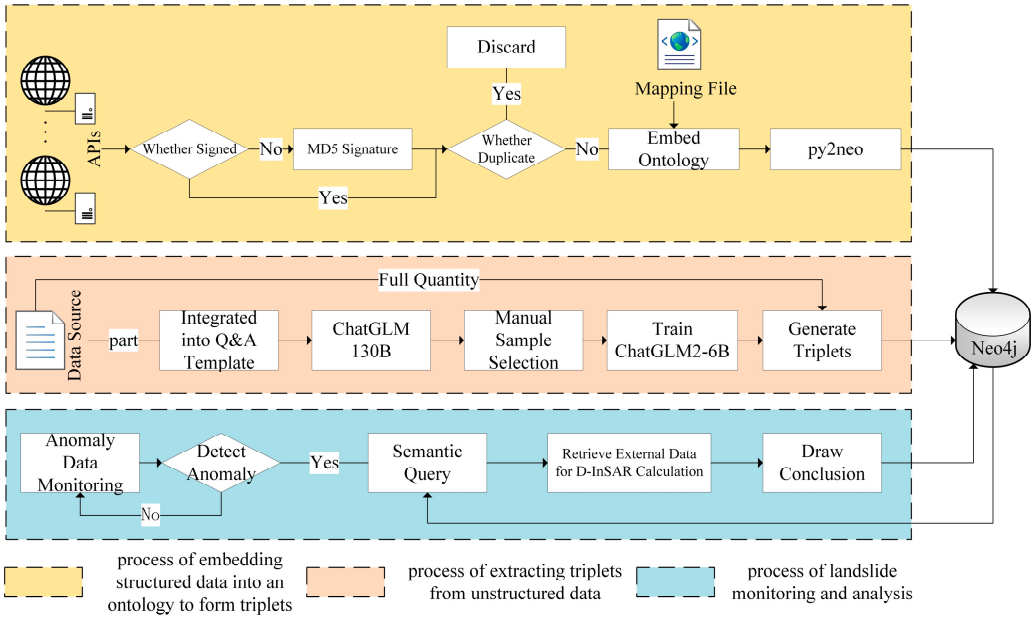


Figure 2. Overall flowchart of landslide knowledge graph monitoring model.

2.3.1. Ontology Construction

The construction of entities in knowledge graphs involves expressing and storing real-world objects, concepts, or events in a structured form. This process includes the following steps: defining and identifying entities, ensuring the uniqueness of entities, selecting and defining entity attributes, establishing relationships between entities, and choosing and integrating data sources. Based on these steps, we propose the following three types of entities: (1) landslide-type entities, which include landslide event entity, landslide research, research method, measurement site, precipitation site, meteorological site, Global Navigation Satellite System (GNSS) site, loss, etc.; (2) geographic-type entities, which encompass economic activity, human activity, natural feature, etc.; and (3) remote sensing-type entities, which contain remote sensing processing, remote sensing index, etc. The main ontologies and relationships are shown in Figure 3.

2.3.2. Entity and Relationship Extraction Based on ChatGLM2

ChatGLM2 is based on the General Language Model (GLM) architecture. This architecture integrates autoencoding and autoregressive concepts by randomly deleting continuous tokens from the input text and sequentially reconstructing them. It combines span shuffling and two-dimensional positional encoding techniques, along with variations in the number and length of missing spans, to cleverly pretrain language models for both conditional and unconditional generation tasks. Its training objective is optimized through an autoregressive blank-filling goal. In this study, ChatGLM2 was used as the baseline model and fine-tuned based on preliminary corpora, enabling the model to transform unstructured text into structured triples. P-Tuning-V2 [48] employs reparameterization to enhance the training speed and robustness of P-Tuning [49]. By adding continuous prompts at each layer of the pretrained model, it significantly increases the capacity of continuous prompts, thereby narrowing the performance gap with fine-tuning, especially on small models and challenging tasks. In this study, P-Tuning-V2 is utilized to fine-tune the pretrained model ChatGLM2-6B.

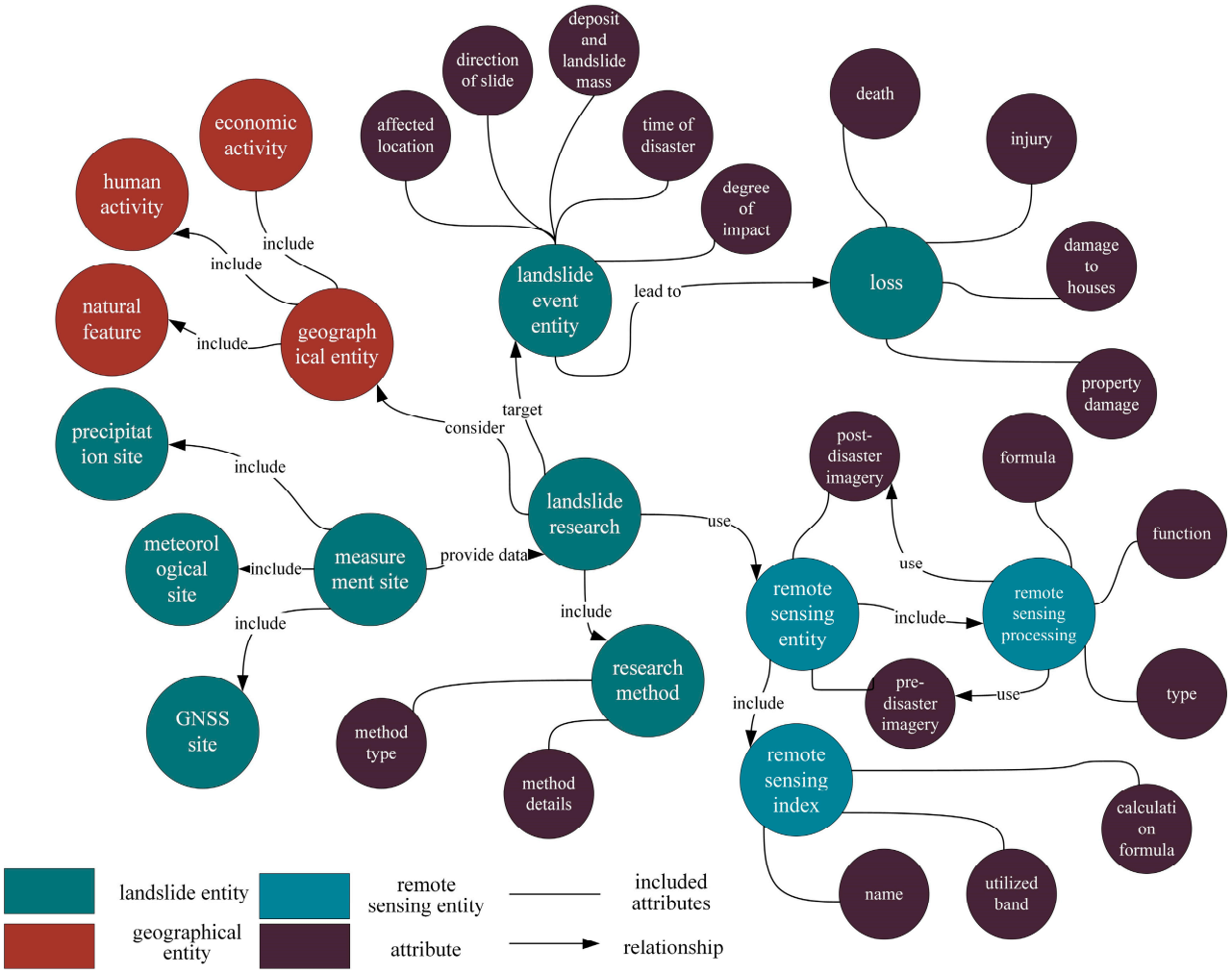


Figure 3. Main ontologies and relationships in the landslide knowledge graph.

In this paper, a question-answering template for generating landslide knowledge graph triples is constructed based on ChatGLM2. By defining roles for ChatGLM2 and providing method examples, we infer the possible triples present in a given text. Our output template is as follows:

$$(\{\text{ Subject }\},\{\text{ Predicate }\},\{\text{ Object }\})<|>\ldots \quad (1)$$

where () represents a triplet, while the content within {} is generated by a large language model. The symbol <|> serves as a delimiter to separate multiple triplets. The ChatGLM2-6B model is fine-tuned to obtain a language model specialized in extracting entities and relationships in knowledge graphs.

Knowledge fusion primarily involves computing the similarity between multiple entities and multiple relationships. Here, we propose a string similarity calculation algorithm that couples the minimum edit distance with the Jaccard coefficient to measure the similarity between multiple entities and relationships. We then set a threshold to perform synonym merging.

The minimum edit distance is a metric used to measure the difference between two strings. It is defined as the minimum number of edit operations required to transform one string into another. These edit operations typically include insertion, deletion, and substitution. Let $d(i,j)$ be the minimum edit distance between strings $word1[0\ldots i)$ and $word2[0\ldots j)$, where $word1[0\ldots i)$ represents the substring of string word1 from position 0 to position i$-$1, and similarly for $word2[0\ldots j)$. Then, $d(i,j)$ can be calculated using the

following recursive relation: (1) Set the initial conditions. For all $0 \leq i \leq len(word1)$, there is $d(i,0) = i$. For all $0 \leq j \leq len(word2)$, there is $d(0,j) = j$. (2) Recursive Formula (4):

$$\begin{cases} d(i,j) = d(i-1,j-1) & ,word1[i-1] = word2[j-1] \\ d(i,j) = \min\{d(i-1,j-1)+1, & ,word1[i-1] \neq word2[j-1] \\ d(i-1,j)+1, d(i,j-1)+1\} & \end{cases} \tag{2}$$

$d(i-1,j-1)+1$ corresponds to substitution operations, $d(i-1,j)+1$ corresponds to deletion operations, and $d(i,j-1)+1$ corresponds to insertion operations.

The Jaccard similarity coefficient is a metric used to measure the similarity between two sets. It is defined as the ratio of the size of the intersection of the two sets to the size of their union. Mathematically, it is expressed as:

$$J(A,B) = \frac{|A \cap B|}{|A \cup B|} \tag{3}$$

A and B are text collections. First, we convert landslide entities into a string-based format for storage. Then, we transform the strings into set forms and use a formula to calculate the Jaccard similarity coefficient $J(A,B)$. Subsequently, we compute the minimum edit distance $d(i,j)$ between the two strings. We then calculate the average of these two coefficients to obtain the distance index $D(word1, word2)$. By setting a distance index threshold, we can merge entities and relationships that exceed this threshold.

2.3.3. Deformation Monitoring Based on D-InSAR

Neo4j graph database is a graph database management system that stores data using graph structures, supporting efficient graph queries and analyses. It offers an intuitive us-er interface and a powerful computation engine, supporting various data input formats and output formats for results. Additionally, it provides a visualization interface for dis-playing results. The triples mentioned in this paper are represented in the form of graphs; therefore, we use Neo4j graph database for landslide knowledge storage and querying.

In this case, the data recommendation and calculation process are illustrated in Figure 4. First, using the Cypher query language of the knowledge graph, we searched for the timing of the landslide disaster, obtaining a time range of one week before and after the disaster event. Concurrently, using the Cypher query language, we searched for the location of the landslide disaster, which in this case was identified as Jishishan Autonomous County. We then queried the county name to obtain its vector boundary. Concurrently, we uploaded the time range and vector boundary to an Application Programming Interface (API) to check for any available imagery. If no images were available, we would expand the time range by another week and continue the search until images were downloaded. The downloaded images were then focused to convert radar echo data into high-resolution images. Next, we registered and superimposed radar images obtained from the same area at different time points to create an interferogram that included information on changes in surface height [50]. We used an interferometric noise removal module to eliminate atmospheric noise and phase noise, thereby improving the quality of the interferogram signal. Subsequently, we used Goldstein filtering [51] to further remove noise from the interferogram. This step helps enhance the coherence of the signal, making subsequent phase unwrapping and deformation analysis more accurate. We then calculated coherence and performed phase unwrapping to facilitate subsequent deformation analysis. If orbital data was available, we refined the orbit to eliminate the influence of orbital errors on the interferogram. After unwrapping, we converted the interferometric phase into actual surface deformation information. Finally, we converted the processed deformation data into a geographic coordinate system and output the processed surface deformation map. The relevant configuration parameters of Differential InSAR (D-InSAR) are shown in Table 3.

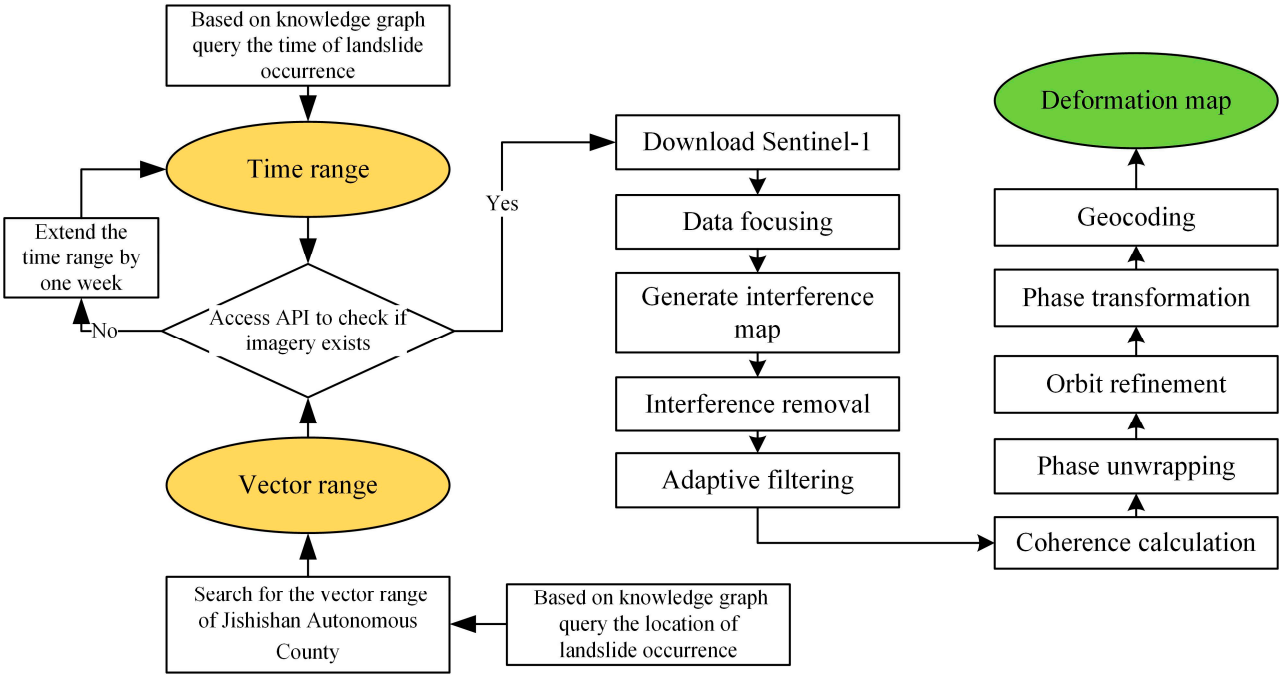


Figure 4. Flowchart of deformation monitoring method based on D-InSAR.

Table 3. Parameter configuration of D-InSAR.

Radar Band	Baseline Parameters	Coherence Threshold	Multi-Looking Factor	Phase Unwrapping Algorithm	Orbit Differential
C-band (Sentinel-1)	7 days	0.5	5	Goldstein Algorithm	Yes

3. Results

3.1. Entity and Relationship Extraction Result

In this example, the monitoring model detected new landslide entities in real-time within the knowledge graph, taking a total of 923 s. This duration excludes the time for text data preprocessing and data transmission, which was 68 milliseconds. The extraction of triplets took 791 s, and knowledge fusion took 131 s. A query was run to retrieve all entities related to this entity. As shown in Table 4, by accessing the background operation logs, we can see that this query took only 14ms and identified a total of 106 related entities and attributes. Among these, there were 17 Landslide Entities, accounting for 16.04%; a total of 12 Geological Environment and Economic Activities Entities, accounting for 11.32%; and 31 Remote Sensing Disaster Monitoring and Image Processing Entities, accounting for 29.24%. The remaining 43.40% of entities and attributes are not based on ontological theory, typically used for supplementary queries and knowledge support, as detailed in Figures A1–A5 in Appendices A–E. Additionally, two computational routes were identified: one based on D-InSAR for deformation calculation, and the other based on knowledge graph queries for image data recommendation.

We conducted a comparative analysis between traditional algorithms and a triplet extraction algorithm based on ChatGLM using the Jaccard index. The analysis included a total of 106 triplets. The results showed that the industry-standard entity extraction algorithm based on spaCy [52] achieved a score of 0.712, while our method scored 0.831. This indicates that our algorithm is more effective at extracting triplets from unstructured data.

Table 4. Details of monitoring model query results.

Total Number of Entities and Attributes	Number of Landslide Entities	Number of Geological Environment and Economic Activities Entities	Number of Remote Sensing Disaster Monitoring and Image Processing Entities	Number of External Operations Involved	Number of Calculation Routes
106	17	12	31	17	2

3.1.1. Landslide Incident Entities

This study encompasses three types of entities: landslide entities, Geological environment and economic activities entities, and Remote sensing disaster monitoring and image processing entities. Figure 5 illustrates a portion of the knowledge graph for landslide entities. This graph is derived from unstructured corpora obtained from public reporting sources. The landslide event entity connects to affected location entities, direction of slide entities, deposit and landslide mass entities, time of disaster entities, degree of impact entities, and loss entities. The loss entity connects to death, injury, damage to houses, and property damage entities. The name attribute of the landslide event entity is "Landslide caused by earthquake in Jishishan County". The landslide research entity points to the landslide event entity with a target relationship. The name attribute of the landslide research entity is the full name of the research. The measurement site entity points to the landslide research entity. We take the landslide event triggered by the earthquake in Gansu on 18 December 2023, as an example. In this instance, only one seismic station is involved, and the earthquake magnitude recorded by the station is 6.2. The landslide event entity points to the research method entity, whose name is "Remote Sensing Monitoring and Geological Interpretation". This entity connects to method type and method details entities, with name attributes of "remote sensing" and "InSAR" respectively.

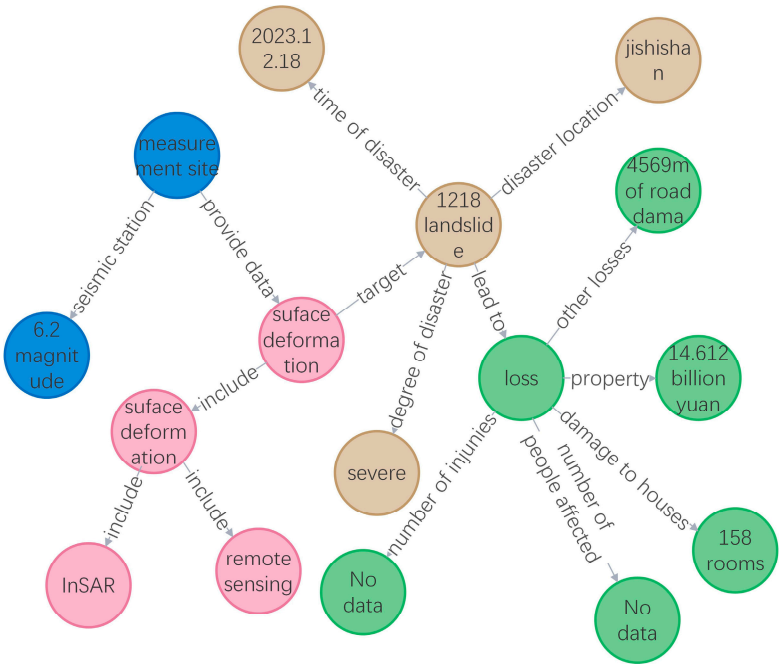


Figure 5. Knowledge graph of jishishan landslide incident entities.

3.1.2. Geological Environment and Economic Activities Entities

In this example, the geological environment and economic activities entities section includes three entities. The rainfall, steep hill, and earthquake entities point to the natural

feature entity. Human activity includes the vegetation, drainage, water storage, blasting, and excavate entities, with blasting and excavate potentially leading to economic activity. The geographical entity includes the economic activity entity. The geological environment and economic activities entities in the Jishishan landslide are shown in Figure 6.

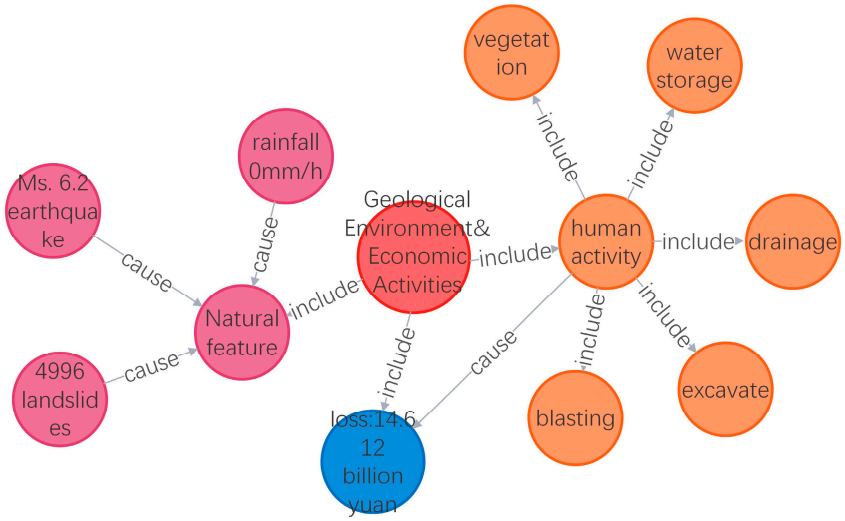


Figure 6. Geological environment and economic activities entities in jishishan landslide.

3.1.3. Remote Sensing Disaster Monitoring and Image Processing Entities

In this example, the included remote sensing entities are shown in Figure 7. The remote sensing entity connects to the remote sensing processing entity and the remote sensing index entity. Both the pro-disaster imagery entity and post-disaster imagery entity are included within the remote sensing entity and the remote sensing processing entity. The remote sensing processing entity further connects to the Slope Calculation entity, Vegetation Index Calculation entity, Filtering Processing entity, and Radiation Correction entity. These entities are associated and operated through the remote sensing processing entity. The remote sensing index entity connects to the Differentiated Vegetation Index entity, Terrain Humidity Index entity, Landslide Hazard Index entity, and Remote Sensing Hydrological Model entity. These are specific index models and calculation methods linked to the remote sensing index entity. Specifically, the slope calculation entity includes three attributes: formula, type, and function. It is worth noting that the slope calculation entity and the vegetation index calculation entity belong to the same type, sharing similar attributes and methods in their processing and calculations. Although the slope calculation entity and the vegetation index calculation entity belong to the same type of entity, they have significant differences in function. The slope calculation entity is primarily used to calculate the slope of the terrain and determine the gradient of the terrain, enabling better understanding and analysis of terrain changes and characteristics. In contrast, the function of the vegetation index calculation entity is to calculate various vegetation indices, which are used to assess the density and health of plant cover. These vegetation indices can help monitor and manage ecosystems, evaluate the impact of environmental changes on vegetation, and support decision-making in agriculture and forestry management. The remote sensing processing entity provides comprehensive support for the analysis and application of remote sensing data by connecting and integrating different types of calculation and processing entities. Meanwhile, the remote sensing index entity offers a wealth of data and analytical tools for geographic information systems and environmental monitoring by linking different index models.

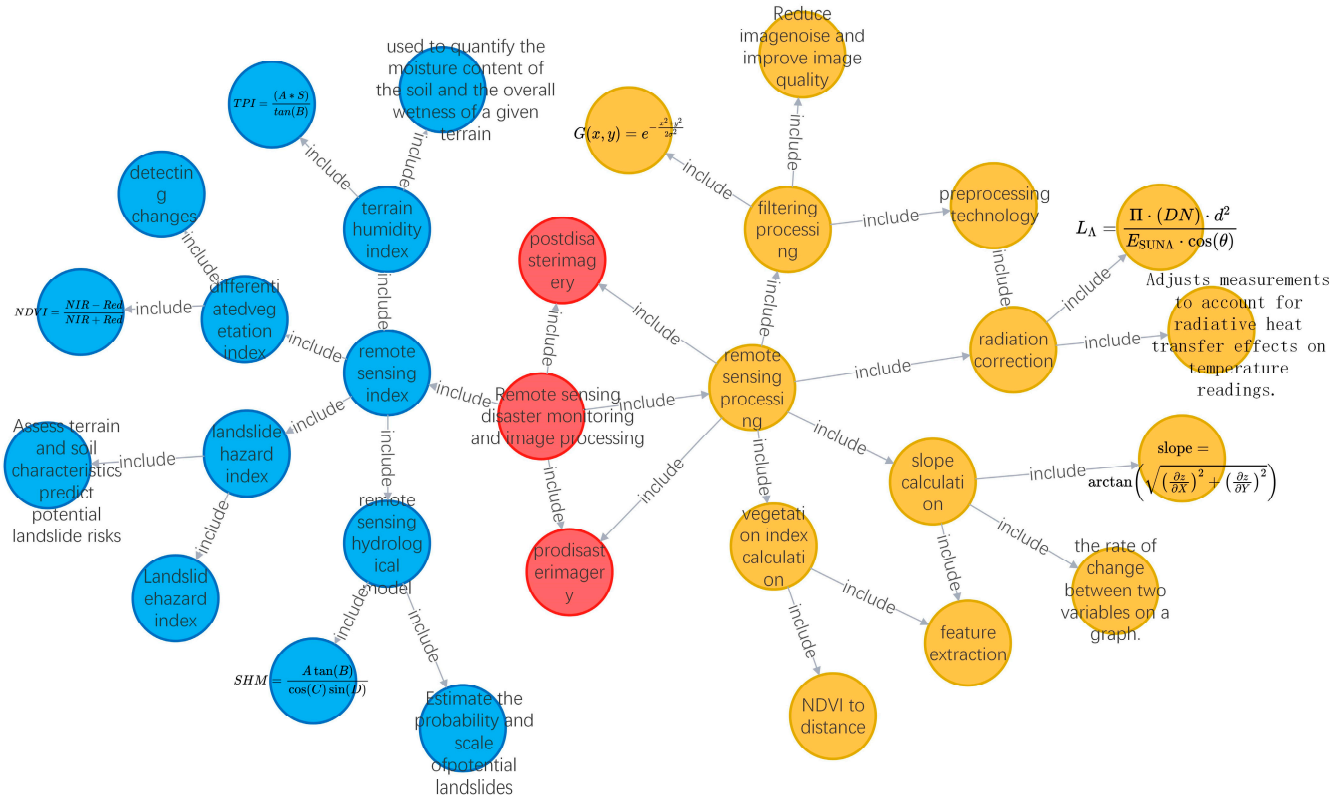


Figure 7. Remote sensing disaster monitoring and image processing entities in Jishishan landslide.

3.2. Deformation Monitoring Results

In this example, the real-time calculation results of the monitoring model are shown in Figure 8. In this model, the monitoring system continuously queries landslide event entities in real-time. When a new landslide occurs, the post-disaster monitoring model is activated. This model inputs all related reports into the pre-trained ChatGLM2 model for entity extraction and normalizes the data for storage in the Neo4J database. For unstructured data, such as remote sensing images, it calls APIs to download images and records their metadata. In this case, after the landslide on 18 December 2023, the knowledge graph-based monitoring model was automatically activated. It downloaded Sentinel-1 images that spatially overlapped with the disaster location (35.70°N, 102.79°E) and were captured before the disaster occurred. Subsequently, the images underwent band merging and import operations. A separate thread was initiated to wait for the next spatially overlapping image captured after the disaster. It is noteworthy that most event entities are generated based on reports, resulting in some delay. Therefore, when the model begins acquiring pre-disaster images, post-disaster images are already being collected. In such cases, the model automatically downloads both pre-disaster and post-disaster images. The model then queries available remote sensing processing methods. Using the network structure, it quickly identifies the need for the D-InSAR method under the landslide node. At this point, the model attempts to invoke the D-InSAR method from the remote sensing processing methods. By querying the nodes connected to the D-InSAR node, it retrieves the metadata required for the method, queries the database for the necessary data, and transfers this data to the working directory. Once data transfer is complete, the D-InSAR workflow proceeds according to preset parameters. The final results are saved to the geographic database, and a new node is added to the Neo4J database to store the result's location. From Figure 8, a substantial area of uplift can be observed between 102°44′ to 102°54′E and 35°42′ to 35°50′N, with the highest uplift reaching 8.784 cm. The southwestern mountains exhibit significant unilateral subsidence. Additionally, there is a significant localized uplift in the northwest direction of the central uplift area, with a maximum uplift of up to

9.662 cm, and the relative error of comparison with the displacement confirmed in the official agency report [53] is 6.17%. Overall, the deformed areas are primarily located among the mountains.

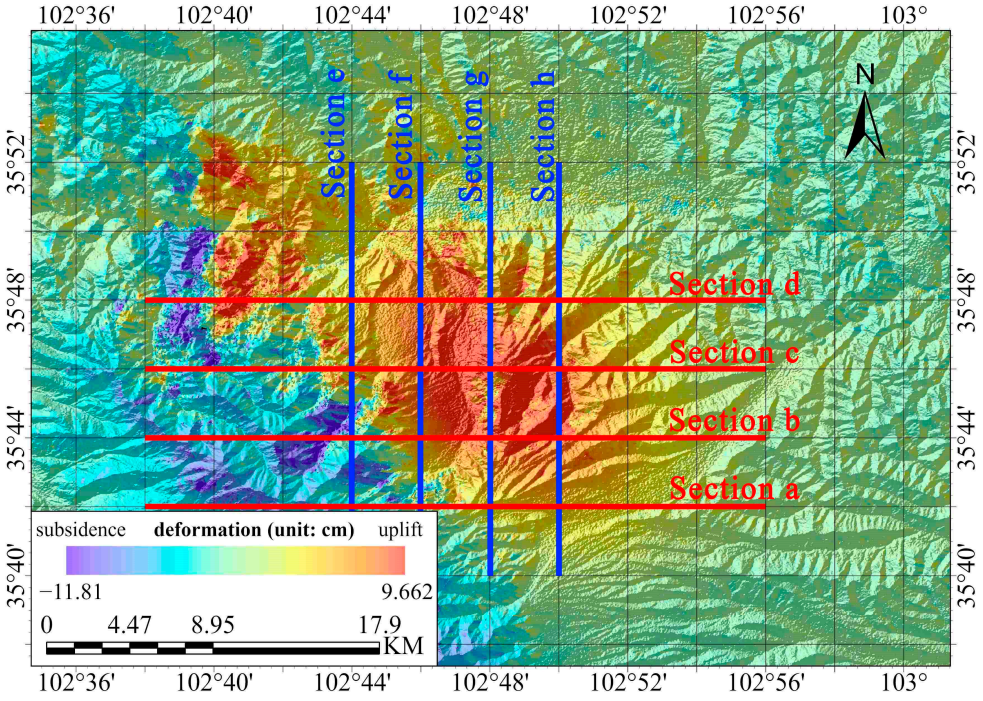


Figure 8. Deformation caused by the earthquake detected by D-InSAR. Sections a to d are vertical profiles, while sections e to h are horizontal profiles.

The monitoring model has integrated advanced profile analysis methods, which automatically push relevant data to researchers when they query specific terrain events. Researchers need only upload vector files of the study area and the target images to the model to easily generate profile graphs. In this study, terrain deformation maps and vector data of the core deformation areas were input, with a horizontal interval of 2′ and a vertical interval of 2′. The generated profile graph (Figure 9) shows that, horizontally, Section f exhibits the most significant deformation, with a fitted line slope of 1.186 and an average deformation of 7.5 cm. Vertically, Section a shows the greatest deformation, with a fitted line slope of 1.032, indicating that horizontal deformation is generally greater than vertical deformation. This may suggest that crustal stress is unevenly distributed horizontally, leading to more significant deformation responses. Specifically, Sections e to f show a distinct west-high-east-low trend, which might be related to underground tectonic activities or historical landslide events, while Section h exhibits more uniform deformation, indicating relatively stable geological conditions, possibly due to more uniform stratigraphic structures and lithological conditions. Additionally, the model automatically performs curve fitting and differentiation to accurately determine the deformation rate at each point. It selects the maximum absolute derivative value in each section and stores it in the landslide knowledge graph. The profile graph's address index and its corresponding derivative values are effectively associated and stored, providing rich secondary data support for subsequent research and monitoring.

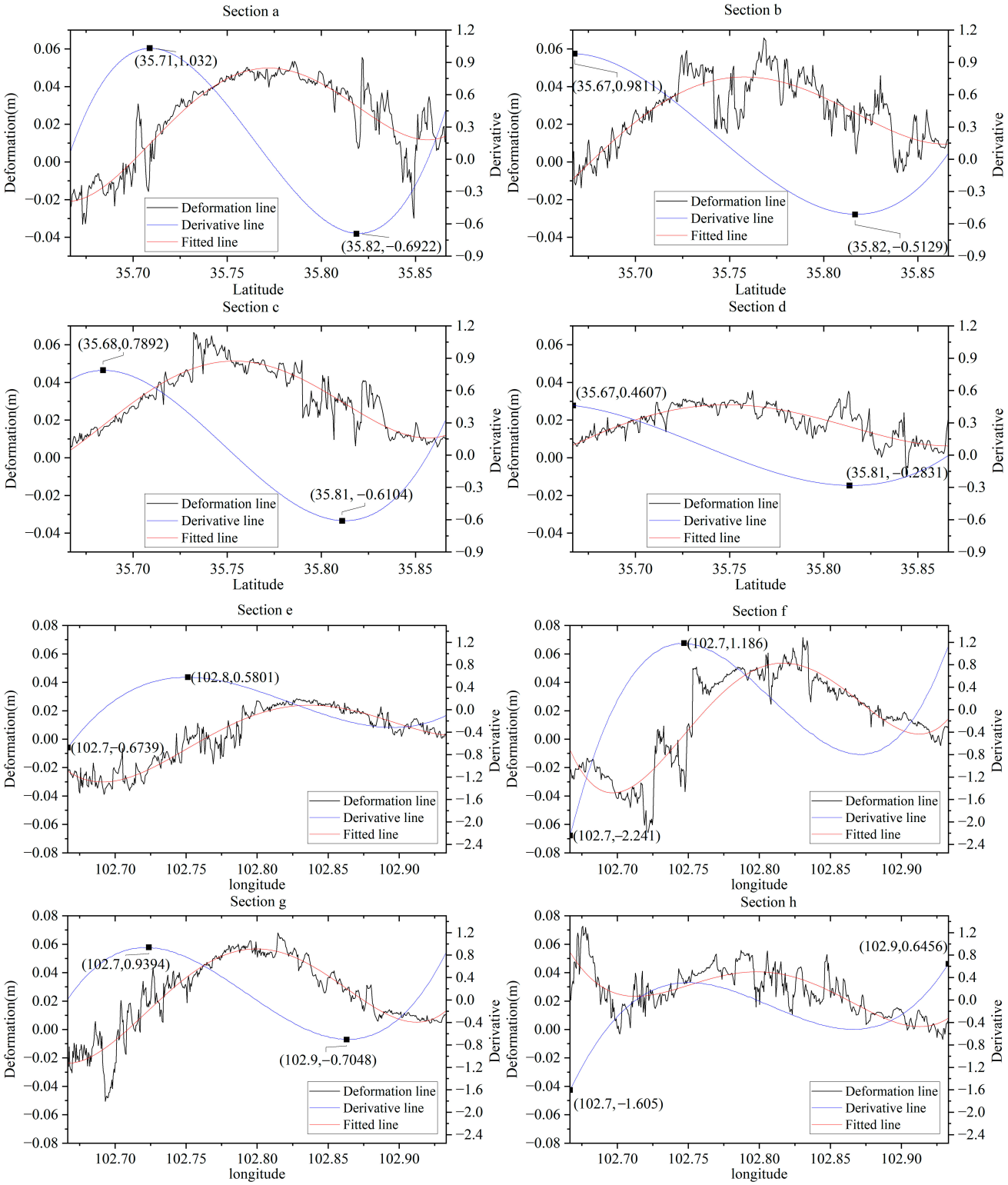


Figure 9. Horizontal and vertical cross-sectional diagrams. The red line represents a quartic fitting curve. The blue line is derived from the differentiation of the fitting curve. (**a**–**d**) are vertical profiles, while sections (**e**–**h**) are horizontal profiles.

Using the landslide knowledge graph-based monitoring model to query landslide disasters associated with this earthquake, we quickly identified the coseismic landslide located in Zhongchuan Township, Haidong City, Qinghai Province. Utilizing the images linked by the model post-disaster, we found pre- and post-disaster Sentinel-2 images of

the affected area (Figure 10). By comparing the pre- and post-disaster results, we observed that the earthquake-induced landslide disaster impacted a large area, with an affected area of 0.3408 square kilometers. The images reveal that the landslide body in the north slid southward, forming a mudflow. The landslide body measures 2632 m in length from north to south and 934 m from east to west. The main affected area is the farmland north of the village, where the mudflow moves southward, overflowing at the bend and the narrow sections of the village, forming deposits.

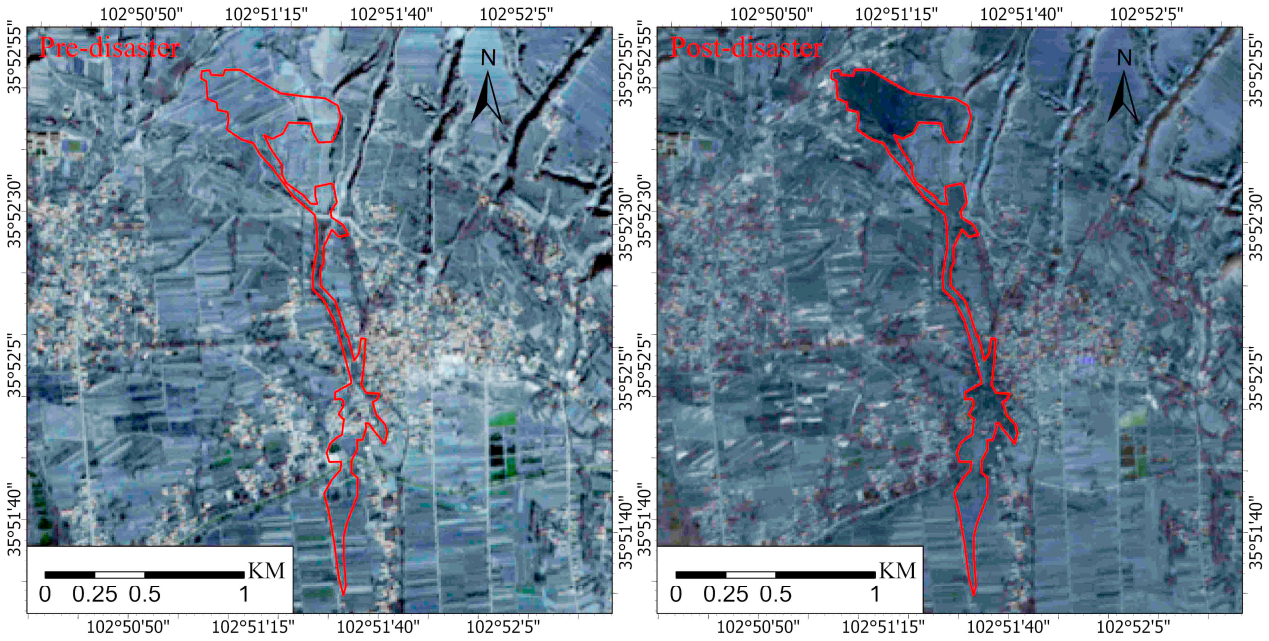


Figure 10. Sentinel-2 image of coseismic landslide triggered by the Jishishan earthquake. This image is synthesized using visible light channels and displayed using the percentage truncation method. The landslide body area is highlighted within the red box. The imaging date of the pre-disaster image is 14 December 2023, and the imaging date of the post-disaster image is 26 December 2023.

Additionally, the model has associated multiple historical landslide sites within the same province as the earthquake, including a mountain in Nanyu Township, Zhouqu County, Gannan Tibetan Autonomous Prefecture, Gansu Province. This area experienced the Zhouqu landslide on 12 July 2018. The main geomorphological units in this area are erosional tectonic mountains and erosional depositional river valley plains. In the erosional tectonic mountains, intense erosion and weathering have led to widespread fragmentation of surface rocks, with abundant cracks and joints, creating conditions conducive to landslides and collapses. Particularly during the rainy season, the risk of mudflows significantly increases. Another associated site is a mountain in Lingtai County, Pingliang City, Gansu Province, where the Lingtai landslide occurred on 3 October 2021, also linked to seismic activity. The landslide at Dongzhuang She in Nandianzi Village is located in a transitional zone between loess hills and erosional depositional river valleys, sharing similar spatial distribution characteristics with the study area. This landslide, dating from the Holocene, has had a long-term impact on the geological environment. The landslide body is composed of multiple sliding blocks, exhibiting distinct cracks and deformation signs that highlight the geological environment's fragility. Meanwhile, the knowledge graph results indicate that various remediation measures have been implemented in the region, including slope cutting and load reduction, pile and panel wall constructions, anchor and grating structures, and water interception and drainage projects, all aimed at enhancing landslide stability and preventing future disasters. This information enables decision-makers to easily investigate the recent earthquake's impact on other historical landslide bodies and provides knowledge of past remedial measures for adoption in neighboring areas.

4. Discussion

4.1. Analysis of the Formation and Regional Impact of Coseismic Landslides

Flow-type landslides are a category of landslides that occur due to soil liquefaction or other forms of enhanced fluidity. These landslides typically take place on steep slopes, where soil layers or loose sediments move rapidly under the influence of gravity. The defining characteristics of flow-type landslides include high flow speeds, the ability to cover extensive areas, and significant destructiveness. The moisture content in the soil is one of the key factors affecting its fluidity; the more saturated the soil, the greater its fluidity. By combining the information provided by imagery and the knowledge graph, we can see that the area near Jishishan is covered with farmland. In the study area, this agricultural field experiences irrigation seepage during the regular irrigation process. Combined with regular rainfall infiltration and groundwater accumulation, this will lead to the regional soil layers being in a high moisture state. The occurrence of the Jishishan earthquake caused local liquefaction of this soil layer, thus accelerating instability and leading to the 1213 landslide. The regional soil layers being in a high moisture state also led to the landslide material being highly water-saturated. However, the landslide mass is located on a slope, affected by gravity, and the highly water-saturated landslide material promoted the formation of mudflows. The mudflow flowed downward, destroying over 4000 m of road and damaging over 200 houses.

4.2. Analysis of Landslide Monitoring Optimization Through Knowledge Graph

Current research has utilized knowledge graphs combined with deep learning neural networks for landslide detection in remote sensing images [54]. These methods perform pixel-level classification on a specific image to identify the precise location of landslides. However, such approaches fail to effectively leverage the existing information within knowledge graphs for extended analysis. Our landslide knowledge graph construction framework is capable of acquiring massive amounts of information from multiple sources and organizing it into a structured format. In this case study, we not only integrated information obtained from optical and radar imagery using the knowledge graph but also incorporated data stored in knowledge bases related to geological environment, economic activities, and historical reports to conduct a detailed analysis of the Jixishan coseismic landslide. Previous research has employed relational graph convolutional networks (RGCNs) to effectively utilize the graph-structured information of landslide cases for monitoring and early warning [55]. However, the reliance on labeled data in this model results in significant resource consumption when processing heterogeneous data. To address this, we introduced ChatGLM2 as our baseline model. By fine-tuning the model, we reduced computational resource requirements, while the strong generalization capability of the large language model enhanced its ability to comprehend the input knowledge.

4.3. Research Contributions and Limitations

In this paper, we present a landslide knowledge graph-based monitoring model designed to integrate and organize public reporting, meteorological, and remote sensing data, and utilizes NLP technology based on ChatGLM2 to transform "un-structured knowledge to structured knowledge" encompassing expert knowledge, media insights, and simulation models. Traditional knowledge graph construction, which relies on manual curation and analysis [56], is inefficient and struggles with large datasets. Our proposed intelligent knowledge graph construction method based on ChatGLM2 leverages the superior natural language understanding capabilities of large language models to accurately extract from diverse unstructured data and to identify non-fixed relationships, resulting in multiple associated triplets. Traditional data storage methods are often isolated, with a lack of effective links between different types of data, which limits the interoperability and depth of analysis [57]. The knowledge graph ontology model, by defining relationships and properties between different data types, not only facilitates organic links between data [58] but also enhances semantic understanding of the data [59], thereby improving the efficiency

and quality of data retrieval and analysis. Through constructing a knowledge graph ontology model, this paper enables regularized storage and fixed relationship linking for input geological data, meteorological data, InSAR image data, optical remote sensing data, public reporting. Based on this knowledge graph, we developed a monitoring model to monitor the entire disaster chain related to landslides. This model calculates pre- and post-disaster ground deformation and updates the graph in real-time with disaster information. Traditional methods often rely on manual analysis and periodic updates [60], which not only result in slower response times but also limit the timeliness and accuracy of data processing and disaster warning. In contrast, our proposed knowledge graph-based monitoring model significantly enhances disaster monitoring efficiency and accuracy through automated and intelligent data processing, achieving these results in just 923 s. This provides robust technical support for disaster prevention and mitigation.

However, there are some limitations to this research. First, the Sentinel-1 data used for deformation monitoring have relatively low spatial resolution, which may compromise the accuracy of earthquake disaster identification. Additionally, the lower resolution of optical imagery provided by Sentinel-2 makes it difficult to discern smaller landslide bodies. Future work should employ remote sensing satellites with higher resolution as the basic data input. Furthermore, integrating ground survey data could more accurately integrate landslide monitoring information into actual land management units, providing more precise monitoring information to land managers. Finally, although we fine-tuned ChatGLM2 using P-Tuning, which reduced the number of trainable parameters to some extent and improved training efficiency, large language models inherently consume significant resources. In future research, we may consider employing model compression techniques, such as quantization and pruning, or introducing more efficient training strategies to further reduce the computational complexity and resource consumption of the model. Further development and application of this method will significantly enhance the timeliness and accuracy of disaster response.

5. Conclusions

This study utilizes the ChatGLM2 to perform triplet extraction on diverse multi-source unstructured data and constructs knowledge linking rules based on ontological theory. It enables real-time extraction and integration of knowledge from government reports, media information, and literary resources to build a knowledge graph monitoring model for landslide disaster surveillance. Taking the Jishishan coseismic landslide as a case study, the research yields the following conclusions:

(1). The query for this event was executed in 14ms, identifying 106 related entities and attributes. Of these, Landslide Entities comprised 16.04%; Geological Environment and Economic Activities Entities accounted for 11.32%; and Remote Sensing Disaster Monitoring and Image Processing Entities represented 29.24%. Additionally, two analytical pathways were generated: one for deformation calculation using D-InSAR, and another for recommending imagery data based on knowledge graph queries.

(2). The area ranging from 102°44′ to 102°54′ longitude and 35°42′ to 35°50′ latitude shows a significant uplift, with a maximum of 8.784 cm. There is notable unilateral subsidence in the mountains to the southwest. Beyond the central uplift zone, significant local uplift occurred to the northwest, reaching up to 9.662 cm.

(3). The northern landslide mass slid southward. The area affected by the co-seismic landslide primarily includes farmland and villages, covering an area of 0.3408 square kilometers.

(4). This landslide was triggered by the rapid liquefaction of the water-containing soil layer due to an earthquake, causing instability. Coupled with topographical factors, a large mixture of soil and rocks with water rapidly slid down the slope, forming a debris flow that destroyed over 4000 m of road and damaged over 200 houses.

(5) The maximum horizontal deformation occurs at the 102°46′ section, with a fitted line slope of 1.186, while the greatest vertical deformation is observed at the 35°42′ section,

with a slope of 1.032. This discrepancy indicates that crustal stress is unevenly distributed in the horizontal direction, leading to more significant deformation responses.

Author Contributions: Conceptualization, H.Y. and Z.W.; methodology, H.Y., Z.W. and C.L.; validation, C.L. and H.Y.; writing—original draft, Z.W.; writing—review and editing, H.Y., Y.C. and B.Y.; supervision, H.Y., Y.C., Q.L. and Z.D.; project administration, B.Y., H.Y. and B.Y.; funding acquisition, H.Y. All authors have read and agreed to the published version of the manuscript.

Funding: This research was supported by the National Key Research and Development Program of China (grant number 2022YFC3004402) and the Henan Provincial Key Research and Development Program (221111321100).

Data Availability Statement: Data are contained within the article.

Acknowledgments: We are grateful to the editors and anonymous reviewers for their thoughtful comments.

Conflicts of Interest: Author Bo Yu was employed by the company CEC Guiyang Exploration and Design Research Institute Co. The remaining authors declare that the research was conducted in the absence of any commercial or financial relationships that could be construed as a potential conflict of interest.

Appendix A

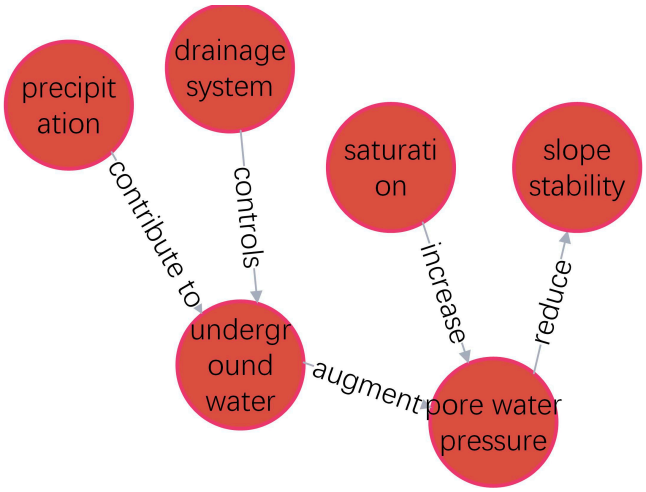


Figure A1. Hydrogeological knowledge graph.

Appendix B

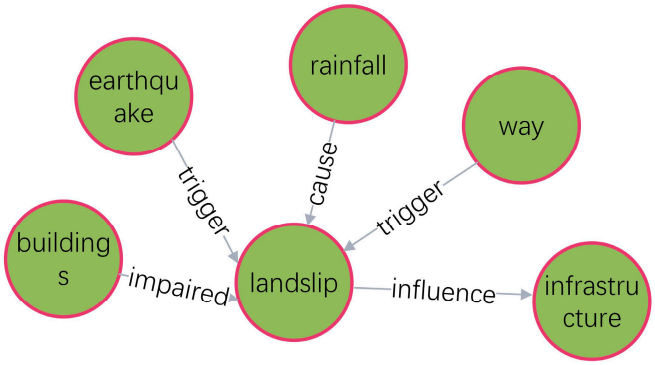


Figure A2. Geohazard knowledge graph illustrating the factors and effects related to landslips, including triggers like earthquakes and rainfall, and their impact on buildings and infrastructure.

Appendix C

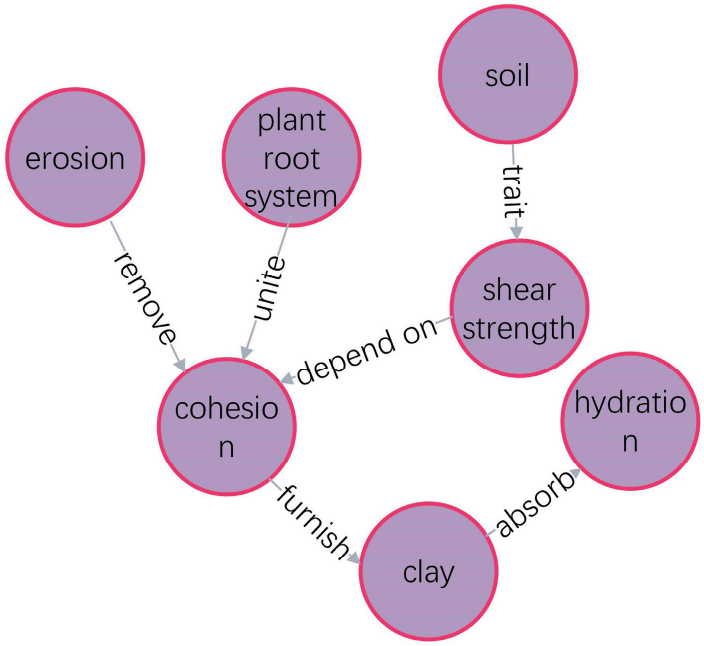


Figure A3. Soil mechanics knowledge graph illustrating the relationships between cohesion, shear strength, and factors such as plant root systems, clay, and erosion.

Appendix D

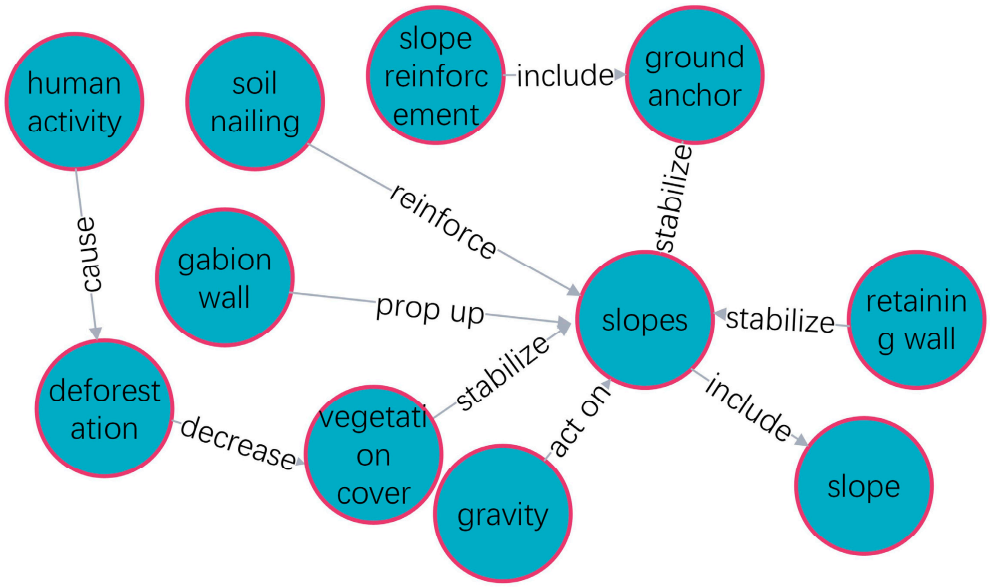


Figure A4. Slope stabilization knowledge graph illustrating the factors and methods involved in reinforcing and stabilizing slopes, including the effects of human activity, deforestation, and various reinforcement techniques.

Appendix E

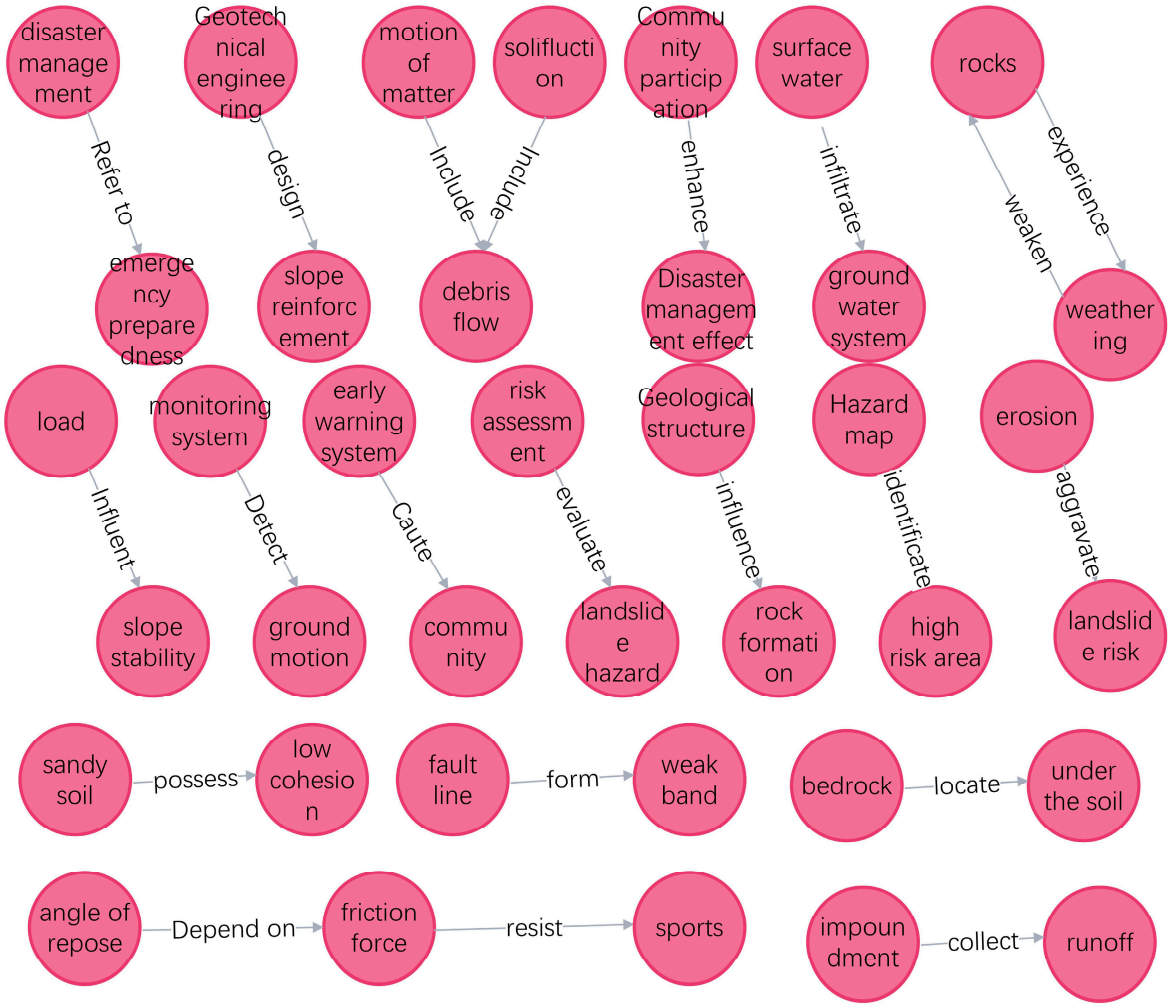


Figure A5. Other Unclassified Knowledge Graphs.

References

1. Kim, T.-H.; Youn, J. A Study on the System Improvement for Efficient Management of Large-Scale Complex Disaster. *Korea Acad. -Ind. Coop. Soc.* **2018**, *19*, 176–183. [CrossRef]
2. Coronese, M.; Lamperti, F.; Keller, K.; Chiaromonte, F.; Roventini, A. Evidence for Sharp Increase in the Economic Damages of Extreme Natural Disasters. *Proc. Natl. Acad. Sci. USA* **2019**, *116*, 21450–21455. [CrossRef] [PubMed]
3. Thomas, V.; Albert, J.; Hepburn, C. Contributors to the Frequency of Intense Climate Disasters in Asia-Pacific Countries. *Clim. Chang.* **2014**, *126*, 381–398. [CrossRef]
4. Jones, P.; Mann, M. Climate over Past Millennia. *Rev. Geophys.* **2004**, *42*, 2. [CrossRef]
5. Tyagi, S.; Garg, N.; Paudel, R. Environmental Degradation: Causes and Consequences. *Evropejskij Issledovatel'* **2014**, *81*, 1491–1498. [CrossRef]
6. Kumar, V.; Kumar, P.; Singh, J. Environmental Degradation Causes and Remediation Strategies. In *Environmental Degradation: Causes and Remediation Strategies*; Agriculture and Environmental Science Academy: Haridwar, India, 2020. [CrossRef]
7. Ferreira, C.; Walsh, R.; Ferreira, A. Degradation in Urban Areas. *Curr. Opin. Environ. Sci. Health* **2018**, *5*, 19–25. [CrossRef]
8. Li, J.-Z.; Li, S.; Wang, W.; Rao, L.; Liu, H. Are People Always More Risk Averse after Disasters? Surveys after a Heavy Snow-Hit and a Major Earthquake in China in 2008. *Appl. Cogn. Psychol.* **2011**, *25*, 104–111. [CrossRef]
9. Yin, Y.; Wang, F.; Sun, P. Landslide Hazards Triggered by the 2008 Wenchuan Earthquake, Sichuan, China. *Landslides* **2009**, *6*, 139–152. [CrossRef]
10. Zhang, X.; Sheng, W.; Qi, S. Hazards and Reflection on Fangshan District Extreme Rainstorm of July 21, 2012, the Urban Mountainous Region of Beijing, North China. *Nat. Hazards* **2018**, *94*, 1459–1461. [CrossRef]
11. Kirschbaum, D.; Stanley, T.; Zhou, Y. Spatial and Temporal Analysis of a Global Landslide Catalog. *Geomorphology* **2015**, *249*, 4–15. [CrossRef]

12. Alexander, D. Disaster and Emergency Planning for Preparedness, Response, and Recovery. In *Oxford Research Encyclopedia of Natural Hazard Science*; Oxford University Press: Oxford, UK, 2015. [CrossRef]
13. Lin, Q.; Wang, Y. Spatial and Temporal Analysis of a Fatal Landslide Inventory in China from 1950 to 2016. *Landslides* **2018**, *15*, 2357–2372. [CrossRef]
14. Dai, F.C.; Lee, C.F.; Ngai, Y.Y. Landslide Risk Assessment and Management: An Overview. *Eng. Geol.* **2002**, *64*, 65–87. [CrossRef]
15. Li, T. *Landslide Hazards and Their Mitigation in China*; Science Press: Beijing, China, 1992.
16. Bragagnolo, L.; Silva, R.M.D.; Grzybowski, J. Landslide Susceptibility Mapping with r.Landslide: A Free Open-Source GIS-Integrated Tool Based on Artificial Neural Networks. *Environ. Model. Softw.* **2020**, *123*, 104565. [CrossRef]
17. Venkatesan, M.; Prabhavathy, P. Big Data Computation Model for Landslide Risk Analysis Using Remote Sensing Data. In *Big Data Analytics for Satellite Image Processing and Remote Sensing*; IGI Global: Hershey, PA, USA, 2018; pp. 22–33. [CrossRef]
18. Zhang, Y.; Zhu, J.; Zhu, Q.; Xie, Y.; Li, W.; Fu, L.; Zhang, J.; Tan, J. The Construction of Personalized Virtual Landslide Disaster Environments Based on Knowledge Graphs and Deep Neural Networks. *Int. J. Digit. Earth* **2020**, *13*, 1637–1655. [CrossRef]
19. Piletski, I.I.; Batura, M.; Shylin, L.Y. Graph Technologies in an Intelligent System of Complex Analysis of Data from Internet Sources. *Dokl. BGUIR* **2020**, *18*, 89–97. [CrossRef]
20. Tran, H.N.; Takasu, A. Analyzing Knowledge Graph Embedding Methods from a Multi-Embedding Interaction Perspective. *arXiv* **2019**, arXiv:1903.11406.
21. Jie, L.; Feng, Z.; Zhang, M.; Jing, F.; Guo, Q. Review of Knowledge Graph and Its Vertical Applications in Industry. In Proceedings of the 2023 42nd Chinese Control Conference (CCC), Tianjin, China, 24–26 July 2023; pp. 5151–5157. [CrossRef]
22. Qingjie, L.; Lingyu, X.; Jie, Y.; Lei, W.; Yunlan, X.; Sui-xiang, S.; Yang, L. Research on Domain Knowledge Graph Based on the Large Scale Online Knowledge Fragment. In Proceedings of the 2014 IEEE Workshop on Advanced Research and Technology in Industry Applications (WARTIA), Ottawa, ON, Canada, 29–30 September 2014; pp. 312–315. [CrossRef]
23. Wang, C.; Yu, H.; Wan, F. Information Retrieval Technology Based on Knowledge Graph. In Proceedings of the 2018 3rd International Conference on Advances in Materials, Mechatronics and Civil Engineering, Hangzhou, China, 13–15 April 2018; pp. 291–296. [CrossRef]
24. Hao, Y.; Zhang, Y. Research on Knowledge Retrieval by Leveraging Data Mining Techniques. In Proceedings of the 2010 International Conference on Future Information Technology and Management Engineering, Changzhou, China, 9–10 October 2010; Volume 1, pp. 479–484. [CrossRef]
25. Wang, N.; Haihong, E.; Song, M.; Wang, Y. Construction Method of Domain Knowledge Graph Based on Big Data-Driven. In Proceedings of the 2019 5th International Conference on Information Management (ICIM), Cambridge, UK, 24–27 March 2019; pp. 165–172. [CrossRef]
26. Purohit, H.; Kanagasabai, R.; Deshpande, N. Towards Next Generation Knowledge Graphs for Disaster Management. In Proceedings of the 2019 IEEE 13th International Conference on Semantic Computing (ICSC), Newport Beach, CA, USA, 30 January–1 February 2019; IEEE: Newport Beach, CA, USA, 2019; pp. 474–477.
27. Pekar, V.; Binner, J.; Najafi, H.; Hale, C.; Schmidt, V.A. Early Detection of Heterogeneous Disaster Events Using Social Media. *J. Assoc. Inf. Sci. Technol.* **2020**, *71*, 43–54. [CrossRef]
28. Hristidis, V.; Chen, S.-C.; Li, T.; Luis, S.; Deng, Y. Survey of Data Management and Analysis in Disaster Situations. *J. Syst. Softw.* **2010**, *83*, 1701–1714. [CrossRef]
29. Bizid, I.; Faïz, S.; Boursier, P.; Yusuf, J.C.M. Integration of Heterogeneous Spatial Databases for Disaster Management. In *Advances in Conceptual Modeling. ER 2013*; Springer: Cham, Switzerland, 2013; pp. 77–86. [CrossRef]
30. Rahman, A. Knowledge Representation: A Semantic Network Approach. In *Handbook of Research on Computational Intelligence Applications in Bioinformatics 2016*; IGI Global: Hershey, PA, USA, 2016; pp. 55–74. [CrossRef]
31. Allen, C.; Balazevic, I.; Hospedales, T.M. On Understanding Knowledge Graph Representation. *arXiv* **2019**, arXiv:1909.11611.
32. Chen, Z.; Wang, Y.; Zhao, B.; Cheng, J.; Zhao, X.; Duan, Z. Knowledge Graph Completion: A Review. *IEEE Access* **2020**, *8*, 192435–192456. [CrossRef]
33. Yu, H.; Li, H.; Mao, D.; Cai, Q. A Relationship Extraction Method for Domain Knowledge Graph Construction. *World Wide Web* **2020**, *23*, 735–753. [CrossRef]
34. Mukherjee, M.; Hellendoorn, V. Stack Over-Flowing with Results: The Case for Domain-Specific Pre-Training over One-Size-Fits-All Models. *arXiv* **2023**, arXiv:2306.03268. [CrossRef]
35. FAISAL, F.; Anastasopoulos, A. Phylogeny-Inspired Adaptation of Multilingual Models to New Languages. *arXiv* **2022**, arXiv:2205.09634. pp. 434–452. [CrossRef]
36. Gili, J.; Corominas, J.; Rius, J. Using Global Positioning System Techniques in Landslide Monitoring. *Eng. Geol.* **2000**, *55*, 167–192. [CrossRef]
37. Rajapakse, R. 19—Geotechnical Instrumentation. In *Geotechnical Engineering Calculations and Rules of Thumb*; Elsevier: Amsterdam, The Netherlands, 2008; pp. 269–272. [CrossRef]
38. Wang, S.; Yang, B.; Zhou, Y.; Wang, F.; Zhang, R.; Zhao, Q. Three-Dimensional Information Extraction from GaoFen-1 Satellite Images for Landslide Monitoring. *Geomorphology* **2018**, *309*, 77–85. [CrossRef]
39. Bellotti, F.; Bianchi, M.; Colombo, D.; Ferretti, A.; Tamburini, A. Advanced InSAR Techniques to Support Landslide Monitoring. In *Mathematics of Planet Earth: Proceedings of the 15th Annual Conference of the International Association for Mathematical Geosciences, Madrid, Spain, 2–6 September 2013*; Springer: Berlin/Heidelberg, Germany, 2014; pp. 287–290. [CrossRef]

40. Aydin, A.; Akyol, E.; Güngör, M.; Kaya, A.; Taşdelen, S. Geophysical Surveys in Engineering Geology Investigations with Field Examples. In *Handbook of Research on Trends and Digital Advances in Engineering Geology*; IGI Global: Hershey, PA, USA, 2018; pp. 257–280. [CrossRef]
41. Jiao, Y.; Zhao, D.; Ding, Y.; Liu, Y.; Xu, Q.; Qiu, Y.; Liu, C.; Liu, Z.; Zha, Z.; Li, R. Performance Evaluation for Four GIS-Based Models Purposed to Predict and Map Landslide Susceptibility: A Case Study at a World Heritage Site in Southwest China. *CATENA* **2019**, *183*, 104221. [CrossRef]
42. Song, K.-Y.; Oh, H.; Choi, J.; Park, I.; Lee, C.-W.; Lee, S. Prediction of Landslides Using ASTER Imagery and Data Mining Models. *Adv. Space Res.* **2012**, *49*, 978–993. [CrossRef]
43. Rompaey, A.; Govers, G. Data Quality and Model Complexity for Regional Scale Soil Erosion Prediction. *Int. J. Geogr. Inf. Sci.* **2002**, *16*, 663–680. [CrossRef]
44. Lu, P.; Stumpf, A.; Kerle, N.; Casagli, N. Object-Oriented Change Detection for Landslide Rapid Mapping. *IEEE Geosci. Remote Sens. Lett.* **2011**, *8*, 701–705. [CrossRef]
45. Song, Y.; Dai, D.; Hu, C.; Gui, M.; Zan, H.; Zhang, K. Research on Partition Block-Based Multi-Source Knowledge Fusion for Knowledge Graph Construction. In Proceedings of the 2022 International Conference on Asian Language Processing (IALP), Singapore, 27–28 October 2022; pp. 458–463. [CrossRef]
46. Zou, Y.; Qiu, D. Combining Tensor Decomposition and Word Embedding for Asymmetrical Relationship Prediction in Knowledge Graphs. In Proceedings of the 2020 13th International Symposium on Computational Intelligence and Design (ISCID), Hangzhou, China, 12–13 December 2020; pp. 87–90. [CrossRef]
47. Du, Z.; Qian, Y.; Liu, X.; Ding, M.; Qiu, J.; Yang, Z.; Tang, J. GLM: General Language Model Pretraining with Autoregressive Blank Infilling. In Proceedings of the 60th Annual Meeting of the Association for Computational Linguistics, Dublin, Ireland, 22–27 May 2022; Long papers. Volume 1, pp. 320–335.
48. Liu, X.; Ji, K.; Fu, Y.; Tam, W.L.; Du, Z.; Yang, Z.; Tang, J. P-Tuning v2: Prompt Tuning Can Be Comparable to Fine-Tuning Universally Across Scales and Tasks. *arXiv* **2022**, arXiv:2110.07602.
49. Liu, X.; Zheng, Y.; Du, Z.; Ding, M.; Qian, Y.; Yang, Z.; Tang, J. GPT Understands, Too. *arXiv* **2023**, arXiv:2103.10385. [CrossRef]
50. Massonnet, D.; Rossi, M.; Carmona, C.; Adragna, F.; Peltzer, G.; Feigl, K.; Rabaute, T. The Displacement Field of the Landers Earthquake Mapped by Radar Interferometry. *Nature* **1993**, *364*, 138–142. [CrossRef]
51. Goldstein, R.M.; Zebker, H.A.; Werner, C.L. Satellite Radar Interferometry: Two-Dimensional Phase Unwrapping. *Radio Sci.* **1988**, *23*, 713–720. [CrossRef]
52. Luo, R.; Xu, J.; Zhang, Y.; Ren, X.; Sun, X. PKUSEG: A Toolkit for Multi-Domain Chinese Word Segmentation. *arXiv* **2019**, arXiv:1906.11455.
53. Institute of Geophysics, C.E.A. Technical Support Brief on the 6.2 Magnitude Earthquake in Jishishan County, Linxia Prefecture, Gansu on 18 December, 2023. Available online: https://www.cea-igp.ac.cn/kydt/280418.html (accessed on 22 October 2024).
54. Xu, B.; Zhang, C.; Liu, W.; Huang, J.; Su, Y.; Yang, Y.; Jiang, W.; Sun, W. Landslide Identification Method Based on the FKGRNet Model for Remote Sensing Images. *Remote Sens.* **2023**, *15*, 3407. [CrossRef]
55. Bo, J.; Yang, Y.; Xiao, H.; Mai, Z. Research on Landslide Spatial Prediction Method Based on Knowledge Graph. In Proceedings of the Third International Conference on Advanced Algorithms and Signal Image Processing (AASIP 2023), Kuala Lumpur, Malaysia, 30 June–2 July 2023; SPIE: Bellingham, WA, USA, 2023; Volume 12799, pp. 511–519.
56. Wang, P.; Deng, X.; Liu, Y.; Guo, L.; Zhu, J.; Fu, L.; Xie, Y.; Li, W.; Lai, J. A Knowledge Discovery Method for Landslide Monitoring Based on K-Core Decomposition and the Louvain Algorithm. *ISPRS Int. J. Geo Inf.* **2021**, *11*, 217. [CrossRef]
57. Zhou, Y.; Liu, L.; Seshadri, S.; Chiu, L. Analyzing Enterprise Storage Workloads with Graph Modeling and Clustering. *IEEE J. Sel. Areas Commun.* **2016**, *34*, 551–574. [CrossRef]
58. Purohit, S.; Van, N.; Chin, G. Semantic Property Graph for Scalable Knowledge Graph Analytics. In Proceedings of the 2021 IEEE International Conference on Big Data (Big Data), Orlando, FL, USA, 15–18 December 2021; pp. 2672–2677. [CrossRef]
59. Pomp, A.; Lipp, J.; Meisen, T. You Are Missing a Concept! Enhancing Ontology-Based Data Access with Evolving Ontologies. In Proceedings of the 2019 IEEE 13th International Conference on Semantic Computing (ICSC), Newport Beach, CA, USA, 30 January–1 February 2019; pp. 98–105. [CrossRef]
60. Yu, H.; Li, H.; Mao, D.; Cai, Q. A Domain Knowledge Graph Construction Method Based on Wikipedia. *J. Inf. Sci.* **2020**, *47*, 783–793. [CrossRef]

Disclaimer/Publisher's Note: The statements, opinions and data contained in all publications are solely those of the individual author(s) and contributor(s) and not of MDPI and/or the editor(s). MDPI and/or the editor(s) disclaim responsibility for any injury to people or property resulting from any ideas, methods, instructions or products referred to in the content.